Digest Journal of Nanomaterials and Biostructures Vol. 10, No. 4, October - December 2015, p. 1311 - 1327

TANDEM SYNTHESIS OF SOME LOW AND HIGH INDEXED MONOMETALLIC NANOPARTICLES IN POLYOLS, POLY(VINYLPYRROLIDONE), TRISODIUM CITRATE AND DODECANETHIOL MATRICES

J. A. ADEKOYA[a,c*], E. O. DARE[b], K. O. OGUNNIRAN[a], T. O. SIYANBOLA[a], O. O. AJANI[a], C. O. EHI-EROMOSELE[a], I. O. OLANREWAJU[a], N. REVAPRASADU[c]

[a]*Department of Chemistry, Covenant University, P. M. B. 1023, Ota, Ogun State, Nigeria.*

[b]*Department of Chemistry, Federal University of Agriculture, Abeokuta, Nigeria.*

[c]*Department of Chemistry, University of Zululand, Private Bag X1001, Kwa-Dlangezwa 3886,*

Sequential synthesis of some noble metal nanoparticles was successfully carried out by polyol/borohydride or hydrazine reduction in the presence of poly(vinylpyrrolidone), trisodium citrate and dodecanethiol in non-aqueous and aqueous solutions with concomitant precipitation of some high index faceted nanoparticles. The polyols afforded Pt NPs as small as 3.5 nm in diameter, which gradually (over a period of months) self-assembled into nanorods that were 5-6 nm in width and 20-30 nm in length. The formation of low indexed Pt NPs species occurred only at moderate temperature, but Pd high indexed face-centered cubic structures formed at 160 $^{\circ}$C, while Co formed high indexed nanodiscs at 190 $^{\circ}$C with an average diameter of 11.23 nm. The process could be monitored by UV absorption spectrophotometer, powder x-ray diffractometer and transmission electron microscopy (TEM). The polyol was indeed multifunctional: it reduced M^{+} (Co^{2+}, Ni^{2+}, Ru^{3+}, Pd^{2+}, Pt^{4+}), stabilized the obtained M^{0} species and served as a template for the tandem formation of monometallic NPs of different morphology.

(Received September 17, 2015; Accepted November 20, 2015)

Keywords: Monometallic, nanoparticles, Polyol, Dodecanethiol, Trisodium citrate, Low index, High index

1. Introduction

Nanoparticles exhibit new functional properties which are not observed either in the individual molecules or in the bulk metals [1]. Therefore, immense effort has been devoted to the synthesis of a different range of transition metal nanoparticles of varying in size, geometry and morphology because of their potential applications, particularly in catalysis [2], electronics [3], chemical sensing [4], and the life sciences [5]. The size, geometry, and dispersion stability greatly determine the suitability of the nanoparticles in some applications. Synthesis may involve physical means such as photo-reduction [6] and chemical reduction in a liquid phase which has been examined intensively in a laboratory scale because of its mass productivity and size controllability [7].

Recently the physical and chemical synthesis of Pt and Pd based nanoparticles is of interest because of their applications in catalysis [8, 9]. They are very highly active electrocatalysts towards oxygen reduction reactions (ORR), methanol oxidation reactions and ethanol oxidation reactions. The catalytic properties were derived from their surface-to-volume ratio and quantum-

* Corresponding author: joseph.adekoya@covenantuniversity.edu.ng

size effects [9]. Several Pt or Pd nanocatalysts supported on various nanomaterials, typically carbon nanomaterials have found applications in polymer electrolyte membrane fuel cells (PEMFCs). They are increasingly developed in fuel cell (FC) technologies for their commercialization in PEMFCs, direct methanol fuel cells (DMFCs), and direct formic acid fuel cells (DFAFCs) [10].

There has been a series of work done recently to develop cheap and durable sources of synthesis and the utilization of various monometal nanoparticles. Sau and Rogach, 2010 [11] provided a review of colloidal chemical synthetic routes and morphological control of non-spherical noble metal nanoparticles. Yang *et al*. (2008) [12] suggested an overall picture of shaped metal nanoparticles in aqueous solutions. The authors described key parameters such as crystallographically selective adsorbates and seeding processes that have an effect on the final shape of the products. Niemeyer *et al*. [13] revealed that evolutionary optimized biomolecules such as nucleic acids, proteins, etc. were effective as capping agents in the preparation of metal nanostructures with potential applications in biomedicine [14]. To date, Pt and Ni are the most widely used as catalytic materials in fuel cells but their high cost and low durability hinder large-scale application of fuel cell technologies. One promising way to lower the Pt cost is to improve its utilization or dispersion, making the most efficient use of every Pt atom in the catalytic process [15]. The wet chemical precipitation method, which consists of polyol or dodecanethiol hydrolysis of metal ion in organic or aqueous solution, is effective in producing tandem metallic nanostructures with specific physical or chemical properties.

A novel method for synthesis of hydrophilic and hydrophobic Pd nanoparticles via the self-regulated reduction by the reflux of sodium dodecyl sulfate (SDS) solution without additional reduction agents was developed [16]. Pd nanoparticles protected with SDS were synthesized with high activities for catalyzing electroless neutral Ni deposition (END) [17]. Co and Pt nanoparticles have been employed as single domain, high-anisotropy magnetic nanoparticles for magnetic recording due to their intrinsic paramagnetic properties. Whereas, NiO and Pd nanoparticle-based hydrogen sensors have been rudimentary to the development of sensing materials due to their sensitivity, selectivity, low operating temperature fast response and recovery time [18].

The common approaches used for the stabilization of NPs include protection by capping ligands such as polymers or surfactants and dispersion in solid supports such as active carbon, metal oxides, zeolites, or polymer films [19]. This method provides rather stable dispersions of nanoparticles. In this process, various kinds of reduction methods can be utilized. The interaction, possibly the coordination bond formation between metal precursors and stabilizers in the reduction system, is a very important factor to produce stable colloidal dispersions of metal nanoparticles [20].

In this paper, we have successfully synthesized monometal NPs by a direct and efficient wet chemical method via exclusive reduction of $M^{2+}/M^{3+}/M^{4+}$ (M = Co, Ni, Ru, Pd, Pt) by polyol, hydrazine monohydrate or sodium borohydride in the presence of poly(vinylpyrrolidone), trisodium citrate and dodecanethiol organic matrices. The resulting monometallic nanoparticles were found to be easily dispersible in aqueous or organic solvent. There were high indexed faceted structures formed as a result of thermodynamic controlled hydrolysis and condensation processes leading to slow particle growth with resultant size confinement.

2. Experimental

The precipitation method of synthesizing well dispersed and size controlled colloidal nanoparticles via rapid hydrolysis and nucleation deployed in this work was modified from literature [21] under controlled temperature conditions. The reaction mechanism for the formation of sequential monometallic nanoparticles with high indexed faceted structure is shown in Schemes 1-2.

$$Pd - (COH)_{ads} + H_2O \rightarrow Pd + CO_2 + 3H^+ + 3e^- \ldots\ldots\ldots (1)$$

$$2Ni^{2+} + N_2H_5^+ + 5OH^- \rightarrow 2Ni + N_2 + 5H_2O \ldots\ldots\ldots\ldots (2)$$

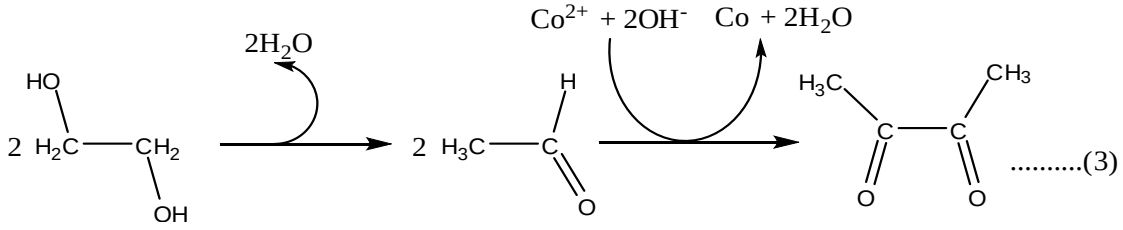

.....(3)

Scheme 1: Showing the reaction mechanisms for the redox system of metal ions In ethylene glycol and hydrazine monohydrate

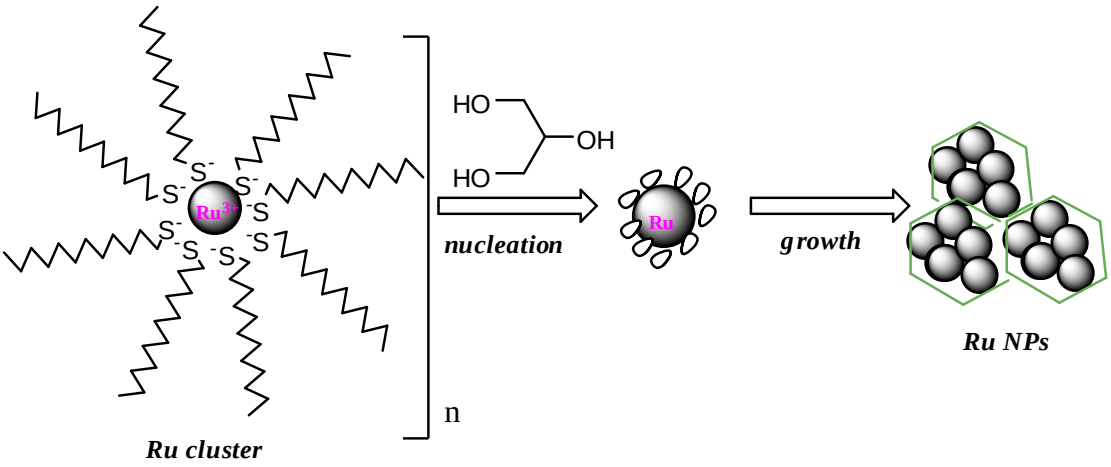

Scheme 2: Thermodynamic controlled growth mechanism of Ru NPs

2.1 Materials

All inorganic salts, solvents and chemical reagents used were analytical grade, and were purchased from Sigma-Aldrich Corporation, UK. They are as follows: tri-*n*-octylphosphine oxide (TOPO), oleic acid (OA), silver nitrate, nickel (II) acetate, cobalt (II) acetate, palladium (II) chloride, platinum (IV) chloride, ruthenium (III) chloride, sodium acetate, glycerol (GLY), ethylene glycol (EG), diethylene glycol (DEG), pentaerythritol (PET), poly(vinylpyrrolidone) (PVP), trisodium citrate (SC), dodecanethiol (DT), sodium borohydride, hydrazine monohydrate, sodium hydroxide, methanol **(**99.5 % w/w), ethanol **(**99.5 % w/w) and toluene.

2.2 Synthesis of monometallic Co, Ni, Pd, Pt and Ru nanoparticles in poly(vinylpyrrolidone), dodecanethiol and trisodium citrate

The monodispersed monometallic Pd nano-sized particles were prepared by the polyol reduction method [22, 23] as follows: 10-15 mL, 99.5% w/w glycerol was measured into a round bottom flask containing a magnetic stirrer, 0.02-0.05 mmol PVP was added, and the apparatus was set up. Then, the mixture was stirred and gradually heated up approximately at a rate of 1.98 $^{\circ}$C/min. to 175 $^{\circ}$C. 0.10-0.18 mmol of $PdCl_2$ was then injected into the hot solution and the reaction was continued for 2 h. Finally, the colour rapidly changed to black. While hot, the resulting Pd sol was washed with methanol several times, centrifuged and redispersed in ethanol. The procedure was repeated for (i) 0.10 mmol $PtCl_4$ (ii) 0.56 mmol $PdCl_2$ in 12 mL DEG at 190 $^{\circ}$C (iii) 0.21 mmol $PtCl_4$ in 12 mL DEG at 190 $^{\circ}$C (iv) 1.06 mmol $Co(CO_2CH_3)_2.4H_2O$ in 12 mL DEG at 190 $^{\circ}$C

(v) 1.86 mmol $Ni(CO_2CH_3)_2.4H_2O$ in 10 mL DEG without PVP at 190 °C (vi) 0.48 mmol $Co(CO_2CH_3)_2.4H_2O$ in EG without PVP at 190 °C, 3 h and (vii) 0.52 mmol $Ni(CO_2CH_3)_2.4H_2O$ in EG without PVP at 190 °C, 3 h.

Similarly, monodispersed Ru nanoparticles in dodecanethiol medium were prepared by the addition of 5-15 mL, 98% w/w dodecanethiol and 121.91-128.733 mM ethanolic sodium acetate solution and the mixture was heated at 2.0 °C/min to 200 °C. Then 0.16-0.34 mmol $RuCl_3$ was injected into the solution phase, followed by hot injection of 5 mL glycerol (as reductant) and the reaction continued for 2 h until the colour rapidly changed to black. While hot, the Ru sol was copiously washed with acetone several times, and centrifuged at 4400 rpm for 10-15 min. to remove excess unreacted stabilizer. The Ru sol was later redispersed in toluene. The procedure was repeated using 5 mL ethylene glycol (as reductant) at 200 °C for 3 h.

Likewise, different monodispersed mono-metal nano-sized particles were prepared in 100 mL deionised water using 0.70 mmol $Co(CO_2CH_3)_2.4H_2O$, 1.05 mmol $Ni(CO_2CH_3)_2.4H_2O$, 0.56 mmol $PdCl_2$ and 0.19 $PtCl_4$ in the presence of 0.04-0.05 mmol PVP and 1.39-1.90 mmol trisodium citrate (SC) at 90 °C with hot injection of 5.0 mL, 23.36-55.51 mM $NaBH_4$ or 3.0 mL $N_2H_4.H_2O$ followed by 8.0 mL, 50 mM NaOH solution (in the case of Ni precursor) for 2 h to produce Co, Ni, Pd and Pt sols respectively. The cooled sols were copiously washed with deionised H_2O several times, and centrifuged at 4400 rpm for 10-15 min. to remove excess unreacted polymer.

Subsequent reactions were carried out in like manner using (i) 33.49-36.72 mmol PET/0.04-0.08 mmol PVP as dual stabilizers and 5-10 mL, 5.39 mM $NaBH_4/N_2H_4.H_2O$ reductant to produce Pd and Pt nanoparticles from 0.54 mmol $PdCl_2$ and 0.29-0.38 mmol $PtCl_4$; (ii) 38.15-40.57 mmol PET (stabilizer) to produce Co and Ni nanoparticles from 1.79 mmol $Co(CO_2CH_3)_2.4H_2O$ and 2.13 mmol $Ni(CO_2CH_3)_2.4H_2O$ respectively. A summary of the stoichiometry ratios of metal precursor/stabilizer or capping agent used to prepare monometallic sols which were redispersed in ethanol/toluene, and the diameter of nanoparticles calculated from *p*-XRD measurement is given in Tables 1 and 2.

2.3 Isolation of monometallic nanoparticles

The centrifuged sols obtained after decantation was redispersed in ethanol and cleaned in ultrasonic bath at 50 °C for 60 minutes before further characterization.

2.4 Characterization

2.4.1 Optical characterization

A Varian Cary 50 Conc UV-Vis spectrophotometer was used to carry out the optical measurements and the samples were placed in silica cuvettes (1 cm path length), using toluene as a reference solvent. A Perkin-Elmer LS 55 Luminescence spectrometer was used to measure the photoluminescence of the particles. The samples were placed in a quartz cuvette (1 cm path length).

2.4.2 Structural characterization

The crystalline phase was identified by X-ray diffraction (XRD), employing a scanning rate of 0.05° min^{-1} in a 2θ range from 20 to 80°, using a Bruker AXS D8 diffractometer equipped with nickel filtered Cu Kα radiation (λ = 1.5406 Å) at 40 kV, 40 mA and at room temperature. The morphology and particle sizes of the samples were characterized by a JEOL 1010 TEM with an accelerating voltage of 100kV, Megaview III camera, and Soft Imaging Systems iTEM software. The detail morphological and structural features were investigated using HRTEM images with a JEOL 2010 TEM operated at an accelerating voltage of 200 kV.

3. Results and Discussion

The stabilized monometallic nanoparticles were found to be very stable both in the liquid and solid phases. The stability was investigated by following the absorbance spectra over extended periods of six months, and reproducible absorption were obtained typical of the metal sol property.

3.1 Optical Properties of Ag/M sols

The Uv/visible absorption spectra of Co, Ni, Pd, Pt monometallic sols stabilized by PVP/GLY at 175 °C, 2 h and Ru sols at 200 °C, 2 h respectively with different metal precursors/ligand mole ratios as shown in Table 1. The optimum stoichiometric ratios for the precipitation reactions which produced the PVP/polyol capped monometallic sols with different metal stabilizing agent mixtures are 1.01:0.05, 1.02:0.04, 0.34:0.02 and 0.10:0.03 for Co/PVP/GLY, Ni/PVP/GLY, Pd/PVP/GLY and Pt/PVP/GLY respectively. At these ratios, colloidal dispersions were formed which were easily re-dispersed in ethanol and the optical absorption of metal sols was conveniently measured.

There was a trend in the shift of absorption maximum observed in PVP/polyol or DT/polyol stabilized monometallic sols (Fig. 1a). The plasmon band (PB) for Co, Ni Pd, Pt and Ru sols occurred at 451, 422, 519, 450 and 443 nm respectively, which is as a result of incident light being scattered and absorbed at resonance frequency due to the collective oscillation of conduction electrons. In all the absorbance spectra (Figs. 1(a-e), the surface plasmon band (SPB) appeared broad with consequent shift towards the visible region. This was observed as result of sole or partly contribution from stabilizing or capping agent made up of polyvinylpyrrolidone (PVP) or dodecanethiol (DT). The absence of peak at 440 and 325 nm characteristic of unreduced Pd(II) indicates complete reduction of the metal ions in Figs. 1(a-e), while the absence of peaks at 378 and 460 nm (Figs. 1(a-e) indicates the reduction of Pt(IV). But Pd and Pt sols show broader absorption in Figures 1(a-e) over the entire range and are dark brown in color. Moreover, shoulders are observed close to 356 nm, Pt PET (Fig. 1d) and 278 nm, Pd PET (Fig. 1d); the origin of these bands is speculated to be due to unreduced Pt and Pd clusters. The effect of change in temperature on the absorbance property of the monometallic sols was also investigated. Figs. 1(a-b) shows that there is a slight blue shift in the broad plasmon band of Ni sol stabilized by PVP/GLY from 422-420 nm for a 15 °C decrease in temperature, this indicates that the growth and Oswald ripening processes are thermodynamically controlled [24].

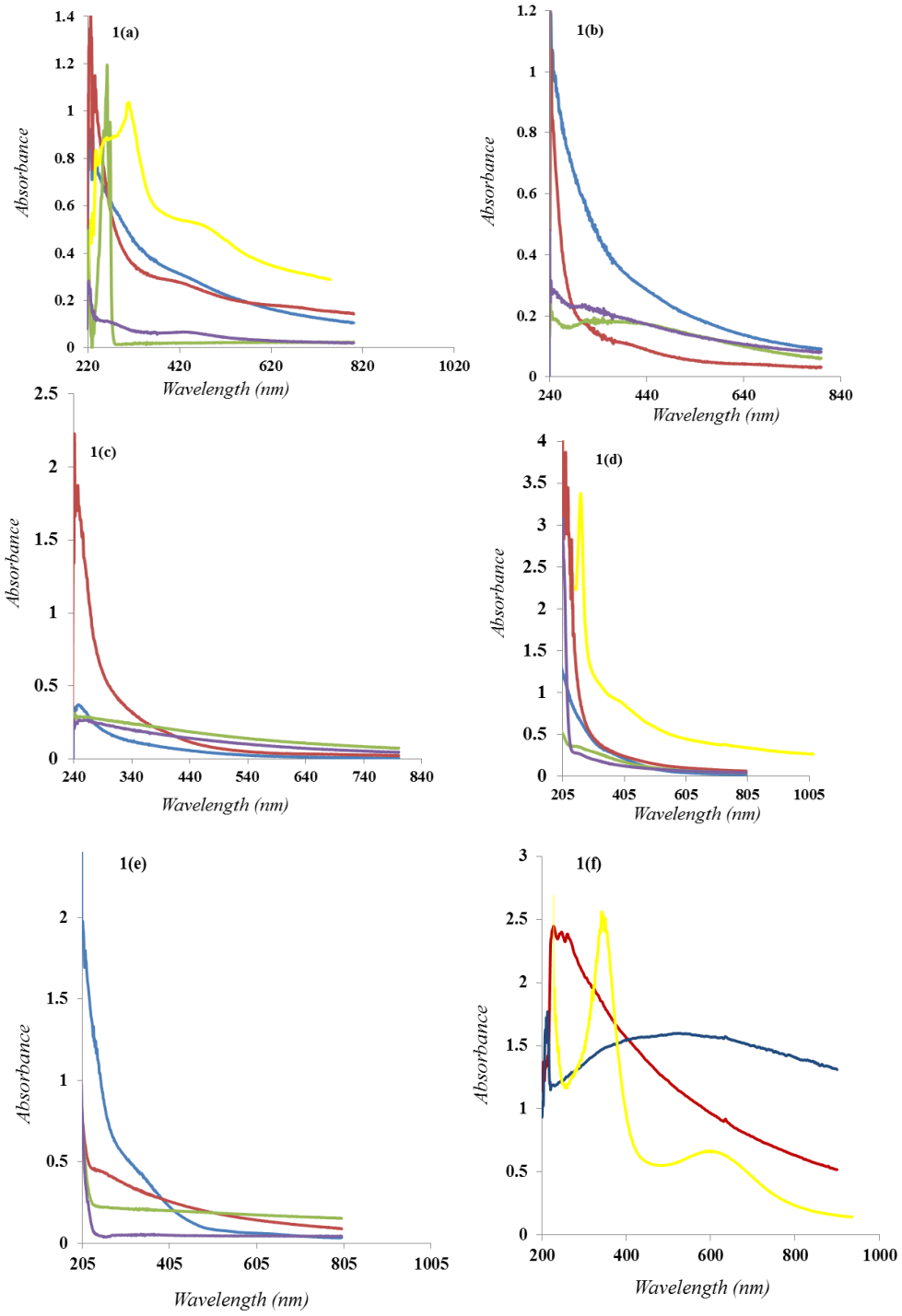

Figure 1: (a) Uv/vis spectra of Co, Ni, Pd and Pt sols stabilized by PVP/GLY at 175 °C, 2 h; Ru sol stabilized by DT/GLY at 200 °C, 2 h ; (b) Uv/vis spectra of monometallic sols stabilized by PVP/GLY at 160 °C, 2 h; (c) Uv/vis spectra of monometallic sols stabilized by PVP/DEG at 190 °C, 2 h;(d) Uv/vis spectra of monometallic sols stabilized by PET at 90 °C, 2 h; (e) Uv/vis spectra of monometallic sols stabilized by PVP/SC in aqueous solution at 90 °C, 2 h; (f) Uv/vis spectra of monometallic sols stabilized by DT/EG, EG at 200 °C, 3 h and 190 °C, 4h respectively

Legends

Abs Ru NPs *Abs Co NPs* *Abs Ni NPs* *Abs Pd NPs* *Abs Pt NPs*

The absorption band gaps of the metal sols estimated by the direct band gap method [25], using the intercepted band edges from Figure 1(a) were found to be 2.75 eV (451 nm, t = 2 h), 2.94 eV (422 nm, t = 2 h), 2.80 eV (443 nm, t=2 h), 2.76 eV (450 nm, t = 2 h) and 2.32 eV (519 nm, t = 2 h) for Co/PVP_{GLY}, Ni/PVP_{GLY}, Ru/DT_{GLY}, Pt/PVP_{GLY} and Pd/PVP_{GLY} stabilized nanoparticles respectively. The absorption edges were completely red-shifted from that of Co, Ni, Ru, Pt and Pd bulk crystals given as 3.17 eV [26, 27], 5.20 eV [28], 3.2 eV [29], 3.0 eV [30, 31] and 7.6 eV [32] respectively. This empirical calculation was also applied to estimate the absorption band gaps of other monometallic nanoparticles stabilized by PVP/DEG, PVP/PET, PVP/SC, DT/EG matrices in Tables 1-2.

The photoluminescence spectroscopy measurement of different as prepared monometallic nanoparticles capped by PVP/polyols was carried out in ethanol, the resulting emission spectrum (Figure 2) was analysed to deduce relative position of emission spectra of the different monometallic sols. Generally, two major emission bands of PVP/polyol capped metallic sols were observed with strong emission peak between 400-417 nm reminiscent of Co, Ni and Ru nanoparticles excited at 340-360 nm, the strong emission band indicates the occurrence of S_1-S_o transition which can be said to be due to stoke's shift. Another relatively strong emission band of Pd and Pt sols occurred between 344-346 nm when excited at 310-315 nm, showed no significant shift in the emission properties which confirms the quantum properties of the as prepared nanosols according to Kasha rule [33] that the emission spectra of potential fluorophores are typically independent of excitation wavelength.

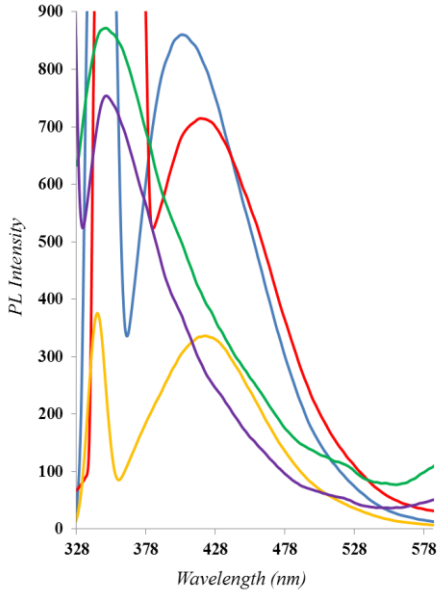

Figure 2: Combined PL emission spectra of monometallic sols stabilized by different polyols

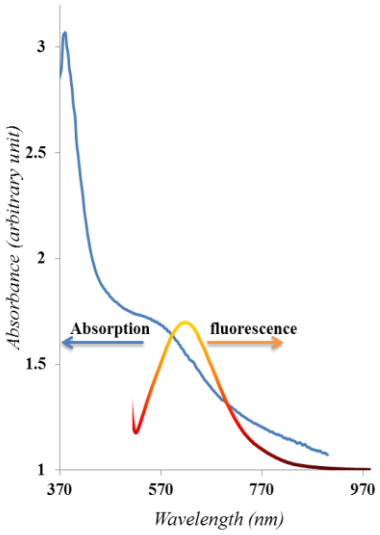

Figure 3: The optical absorption spectrum (blue line) and the emission fluorescence spectrum (orange line) of a toluene solution containing nano-dispersed Ru particles

The optical absorption spectrum and emission fluorescence spectrum of a toluene solution containing nano-dispersed GLY/DT stabilized Ru are shown in Fig. 3. It is well-known that VIIIA-IIB transition metal nanoparticles, exhibit enormous change in their optical absorption spectra when their size is reduced to a few nanometers. The absorption maximum is clearly blue shifted to 443 nm, as compared to the bulk band gap of the tetragonal structure (505 nm, 2.46 eV) which is lattice matched with isostructural RuO_2 [34, 35], which suggests the presence of nanoparticles with size below the bulk exciton dimension of RuO_2. The maximum observed in the spectrum of nano-dispersed GLY/DT passivated Ru is attributed to the lowest electronic transition

occurring in RuO_2 nanocrystallites. On the basis of the effective mass approximation (EMA), the excitonic peak located at 470 nm (Fig. 3) suggesting the presence of RuO_2 nanoparticles with a diameter close to 15.50 nm. Discrepancies between the experimentally measured particle diameter and the predicted one by the EMA have been reported by other authors [36, 37].

The photoluminescence spectrum of the Ru DT/GLY sol (Fig. 3) exhibits a low energy band at 580 nm. The low energy luminescence is due to the mid-gap surface states commonly observed for small RuO_2 clusters. The sharp luminescence band almost overlaps the exciton absorption peak at 470 nm. Based on this, almost a mirror image relationship of the spectral peak positions, the sharp luminescence is attributed to the bound exciton luminescence. The Stokes shift is very minimal, corresponding to very shallow defects. In order to protect the individual crystallites from the chemical degradation and improve their dispersive ability in organic solvents such as thiols and polyols have been introduced into the reaction system. The surface complexation of nanoparticles always provides colloids without detectable luminescence, which is attributed to the ability of complexation to act as hole traps [38, 39], thus preventing any efficient radiative recombination of the excited carriers, especially at room temperature.

Table 1: Summary of the properties of synthesized monometallic nanoparticles in different polyols

Nanoparticles	Temperature of Reaction (°C)	Amount of precursors M_1/M_2/Stabilizer in mmol	d = size of particles (nm)	t=duration of reaction (hour)	Absorbance: λ_{max} (nm)/ band gap (eV)
$Co/PVP/_{GLY}$	175 °C	1.01/0.05	-	2	451/2.75
$Ni/PVP/_{GLY}$	175 °C	1.02/0.04	-	2	422/2.94
$Pd/PVP/_{GLY}$	175 °C	0.34/0.02	-	2	519/2.39
$Pt/PVP/_{GLY}$	175 °C	0.10/0.03	-	2	450/2.76
Ru/DT_{GLY}	200 °C	0.34	-	2	443/2.80
Co/PVP_{GLY}	160 °C	0.36/0.02	-	2	470/2.64
Ni/PVP_{GLY}	160 °C	0.82/0.02	-	2	420/2.96
Pd/PVP_{GLY}	160 °C	0.23/0.01	18.28±5.72	2	436/2.85
Pt/PVP_{GLY}	160 °C	0.11/0.01	9.86±1.58	2	326/3.81
$Co/PVP/_{DEG}$	190 °C	1.06/0.05	-	2	402/3.09
$Ni/PVP/_{DEG}$	190 °C	1.86/0.05	-	2	468/2.65
$Pd/PVP/_{DEG}$	190 °C	0.56/0.03	-	2	474/2.62
$Pt/PVP/_{DEG}$	190 °C	0.21/0.03	-	2	503/2.47
Co/EG	190 °C	0.48	11.23±3.82	4	503/2.47
Ni/EG	190 °C	0.52	106±46.52	4	490/2.53
Ru/DT_{EG}	200 °C	0.16	33.20±5.67	3	387/3.21

Table 2: Summary of the properties of synthesized monometallic nanoparticles in PET and SC

Nanoparticles	Temperature of Reaction in ^{0}C	Amount of precursors M_1/M_2/Stabilizer in mmol	d = size of particle (nm)	t=duration of reaction (hour)	Absorbance: λ_{max} (nm)/band gap (eV)
Co/PET/$_{BH\ (aq)}$	90 $^\circ$C	1.79/38.15	33.43±9.55	2	344/3.61
Ni/PET/$_{BH\ (aq)}$	90 $^\circ$C	2.13/40.57	-	2	345/3.60
Ru/PVP/PET$_{BH\ (aq)}$	90 $^\circ$C	0.28/0.03/23.87	-	4	429/2.89
Pd/PVP/PET/$_{BH\ (aq)}$	90 $^\circ$C	0.54/0.04/36.72	-	2	438/2.84
Pt/PVP/PET/$_{BH\ (aq)}$	90 $^\circ$C	0.29/0.05/36.25	-	2	356/3.49
Co/PVP/SC/$_{BH\ (aq)}$	90 $^\circ$C	0.70/0.04/1.42	-	2	474/2.62
Ni/PVP/$_{NH\ (aq)}$	90 $^\circ$C	2.10/0.03	33.98	2	389/3.19
Pd/ PVP/SC/$_{BH\ (aq)}$	90 $^\circ$C	0.56/0.04/1.39	7.57±1.72	2	515/2.41
Pt/PVP/SC/$_{BH\ (aq)}$	90 $^\circ$C	0.19/0.04/1.90	5.85	2	582/2.13

3.2 Morphology of the monometallic sols

The TEM images of Co nanoparticles (Fig. 4a, b) and (Figure 7a) showed the formation of ethyleneglycol based nanospheres and pentaerythritol based pseudo-cubic structures respectively. The Co nanoparticles in ethylene glycol medium without a stabilizer were monodispersed and uniformly distributed (Fig. 5a), giving an average particle diameter of 11.23±3.82 nm, which was less than the size of Ag nanoparticles (21.7 nm) and Ag-Co nanoparticles (24.9 nm) obtained from TEM measurement in recent work [40].

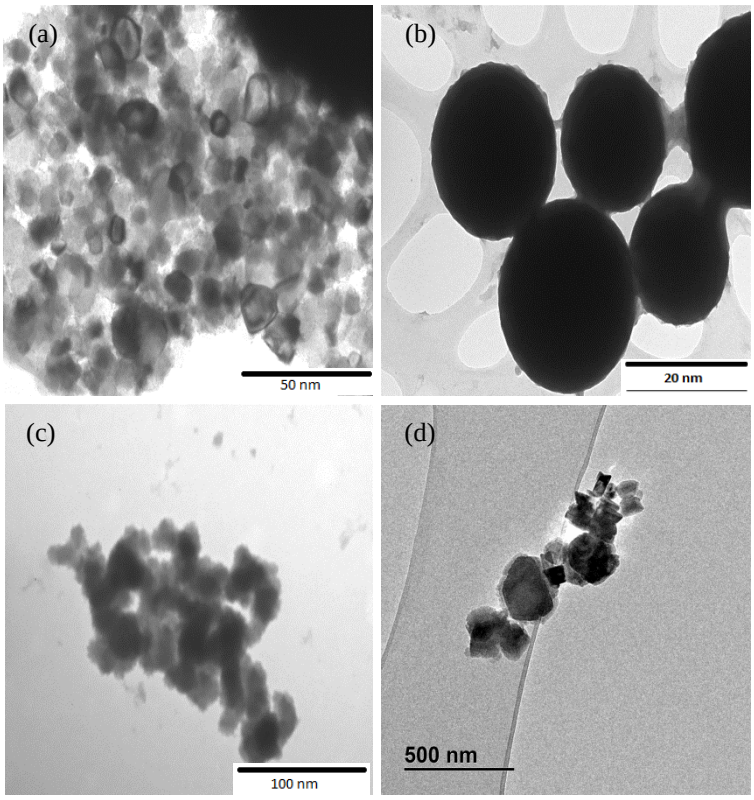

Fig. 4: TEM images (a, b) Co NPs; (c,) Ni NPs stabilized by EG at 190 $^\circ$C, 4h; (d) corresponding HRTEM image of (c)

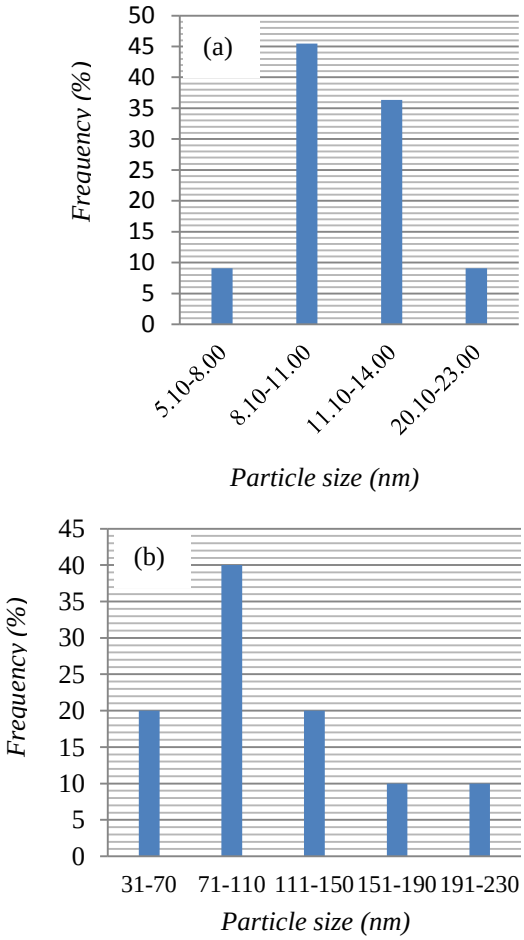

Figure 5: (a) Particle size distribution histogram of Co NPs stabilized by EG
(b) Particle size distribution histogram of Ni NPs stabilized by EG

Although Ni nanoparticles stabilized with PVP/EG at 190 °C, 4h (Figure 4c, d) clearly showed a tendency toward mesoporous aggregation with the presence of face-centered cubic shaped nano-rods produced by anisotropic growth [41], the low index faceted amorphous structure was not compromised, proving that the polyol reduction method could indeed provide quantized particles required for optical, electromagnetic, thermioelectric and catalytic applications. The average diameter was 106±46.52 nm, although agglomerated; the particle size spread (Fig. 5b) shows some degree of homogeneity.

The electron micrographs of monometallic Pd and Pt nanoparticles presented in (Figures 6-8) show the formation of both low and high index faceted nanostructures as a result of lower surface energy [42]. All the nanoparticles were monodispersed, with the exception of Pd NPs stabilized with PVP/GLY at 160 °C, 2h (Figure 6a, b) which showed the presence of different face-centered polycrystalline high indexed cubic structures assigned to the {100}, {111} and {110} planes corresponding to cubic, octahedral and polyhedral spatial geometries respectively [43]. They have an average particle size of 18.28±5.72 nm with the size distribution quite homogenous (Fig. 7a). Whereas, the Pt NPs passivated by PVP/GLY (Fig. 6c, d) showed successful tandem synthesis of monodispersed (Fig. 7b) truncated edge cubic structures with an average diameter of 9.86±1.58 nm.

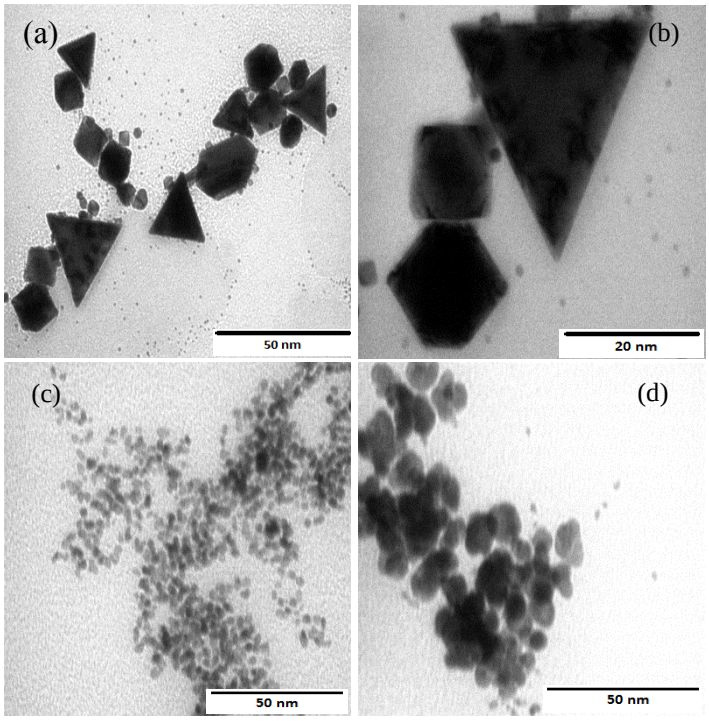

Fig. 6: TEM images (a, b) Pd NPs; (c, d) Pt NPs stabilized by PVP/GLY at 160 °C, 2h.

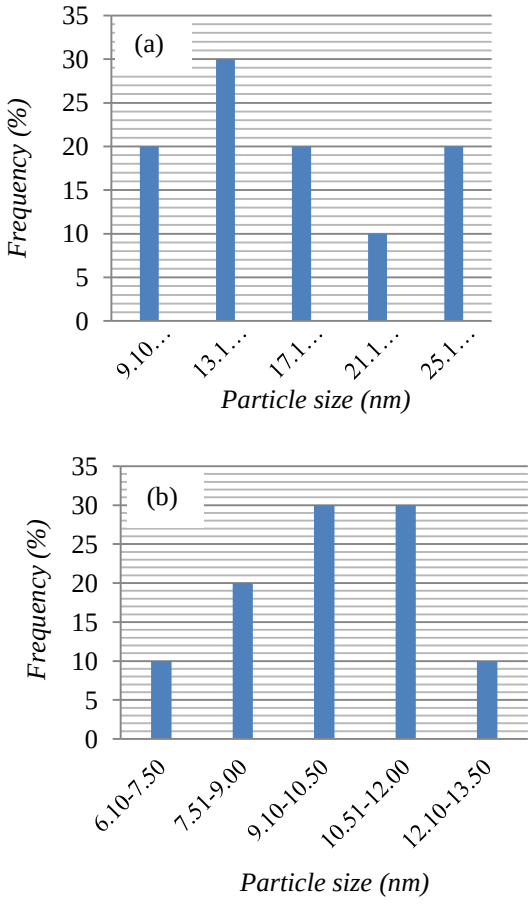

Fig. 7: (a) Particle size distribution histogram of Pd NPs stabilized by PVP/GLY
(b) Particle size distribution histogram of Pt NPs stabilized by PVP/GLY

Moreover, diverse morphologies of Pd and Pt nanoparticles passivated by PVP/SC (Figure 8) were observed. The TEM image indicates the presence of well dispersed (Fig. 9a), crystalline, low indexed structures with truncated edge nanocubes entwined in nanowires (Figure 8a) formed due to diffusion limited growth [44], which occurred as a result of hot solvent segregation of PVP/SC passivated Pd nanoparticles in methanol during the purification and isolation process. The average particle diameter is 7.57±1.72 nm. Similarly, Pt NPs prepared in the same medium produced a network of truncated edge nanocubes (Fig. 8b), nanowire (Fig. 8c) and nanorods (Figure 8d), with some degree of dispersity (Fig. 9b), while the mean particle diameter was 3.67±0.70 nm indicating significant quantum size confinement in the nanoparticles. Moreover, aqueous soluble Co and Ni NPs capped by PET (Fig. 10a, b) produced some quassi or pseudo nanocubes but with some degree of agglomeration in the latter, while the former is monodispersed (Fig. 11a). The mean particle diameter for the aqueous soluble Co NPs was 33.43±9.55 nm. The effect of capping agent on Ru nanoparticles passivated by dodecanethiol (Figure 10c, d) was also found to produce crystalline truncated edge nanocubes with a mean particle size of 33.20 ± 5.67 nm, confirming the occurrence of size confinement effect in the resulting nearly monodispersed Ru NPs (Fig. 11b). Conclusively, the more crystalline phase evolved in glycerol based Pd and Pt nanoparticles due to etching as a result of inclusion of electron withdrawing species Cl^- ion and oxygen [45].

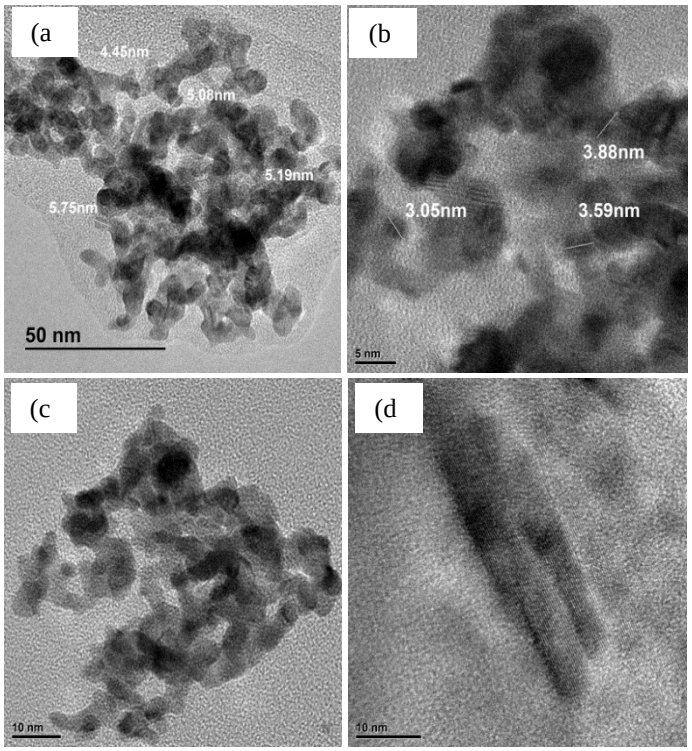

Fig. 8: HRTEM images (a) Pd nanowire; (b) fcc Pt NPs with truncated edges; (c) Pt nanowire; (d) Pt nanorods passivated by PVP/SC at 90 °C, 2h.

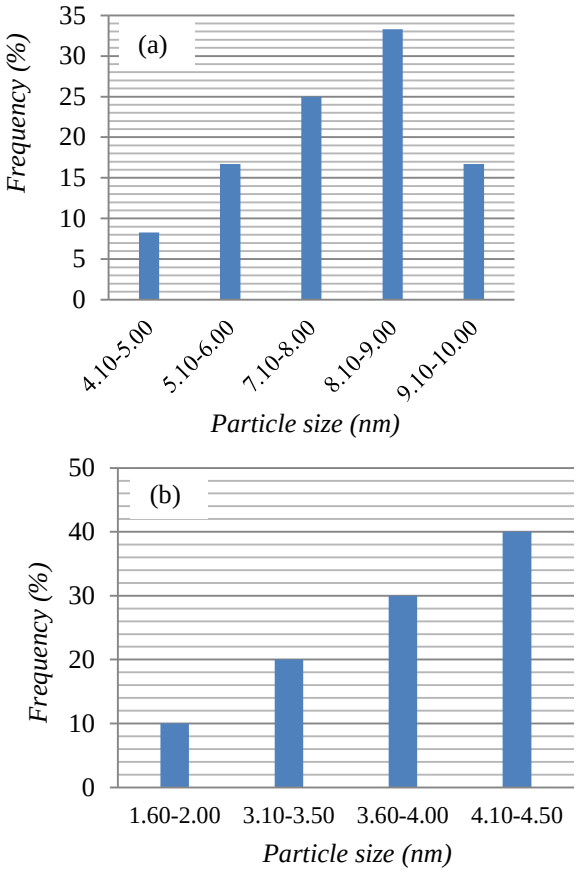

Figure 9: (a) Particle size distribution histogram of Pd NPs stabilized by PVP/SC (b) Particle size distribution histogram of Pt NPs stabilized by PVP/SC

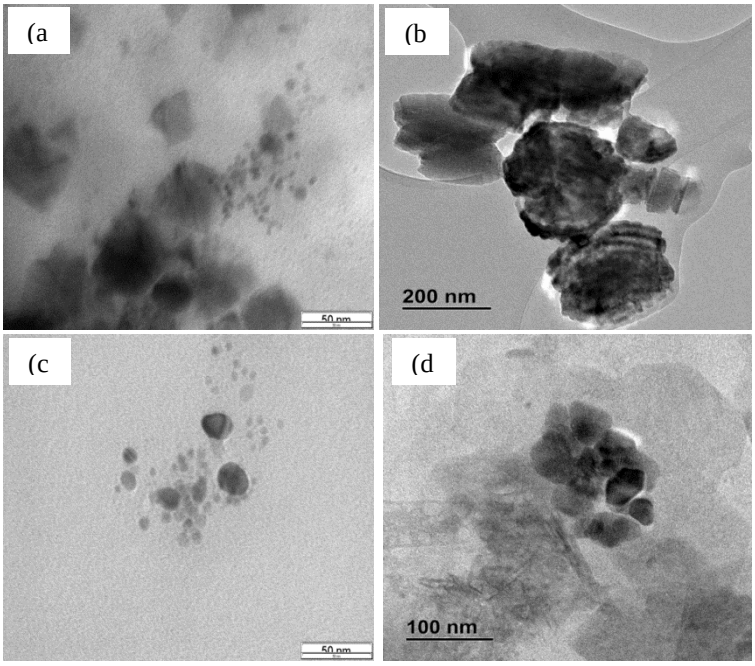

Fig. 10: TEM image (a) Co NPs stabilized by PET, HRTEM (b) agglomerated hcp Ni NPs stabilized by PET at 90 °C, 2h, (c) TEM image of Ru NPs stabilized by DT/EG at 200 °C, 3 h (d) the corresponding HRTEM of (c)

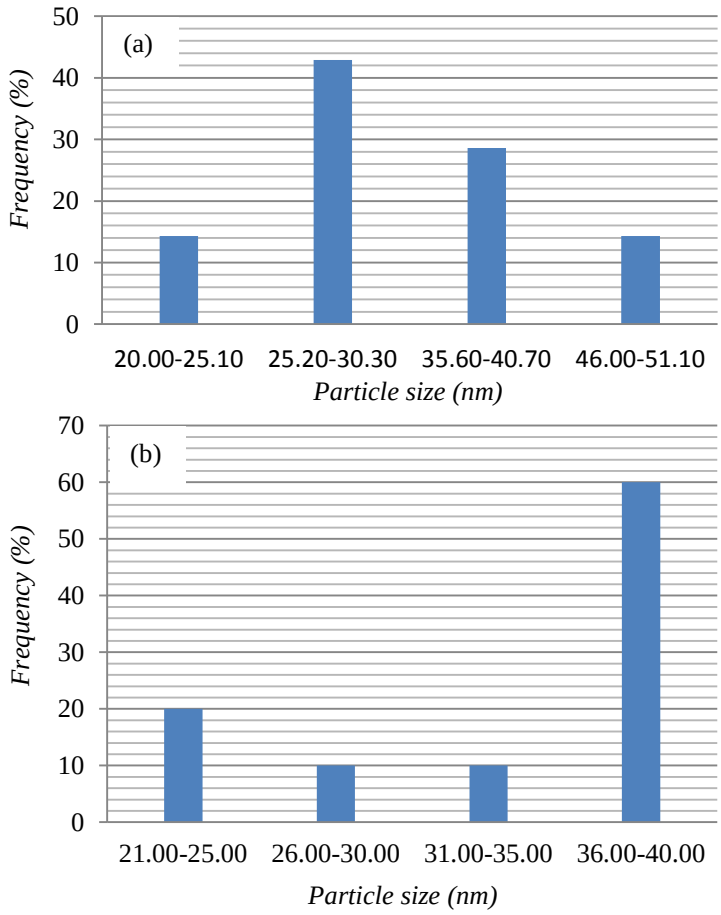

Figure 11: (a) Particle size distribution histogram of Co NPs stabilized by PET (b) Particle size distribution histogram of Ru NPs stabilized by DT/EG

The representative XRD patterns of the prepared monometallic nanoparticles are shown in Figure 12. The result indicate that Ni NPs (Fig. 12a) were highly crystalline, isostructural with $FeTiO_3$ [46, 47] and underwent a nearly complete phase transition from the fcc to the hcp phase through a low temperature hydrazine reduction of Ni(OAc) in the PVP matrix. A medium diffraction peak (2θ = 52.03°) that does not belong to the hcp phase also appear in the XRD pattern, one of the possible explanations for such a peak is the lattice increase of fcc nickel, which may involve the diffusion of carbon atoms into the lattice of nickel [48, 49]. In recent study on the preparation of nickel nanoparticles in polyethylene glycols, hcp nickel nanoparticles were obtained at a higher temperature [50]. The formation of the hcp phase occurring at a higher reaction temperature certainly relates to thermodynamic factors. However, this work has also shown that at low temperature and faster decomposition of nickel precursor could produce a higher concentration of nickel atoms by the hot injection of hydrazine in aqueous solution, which may be thermodynamically favorable for the formation of the hcp phase. The particle size calculated from the most intense peak {015} using the Scherrer programme is 33.98 nm, with the lattice constant at 0.2324 nm.

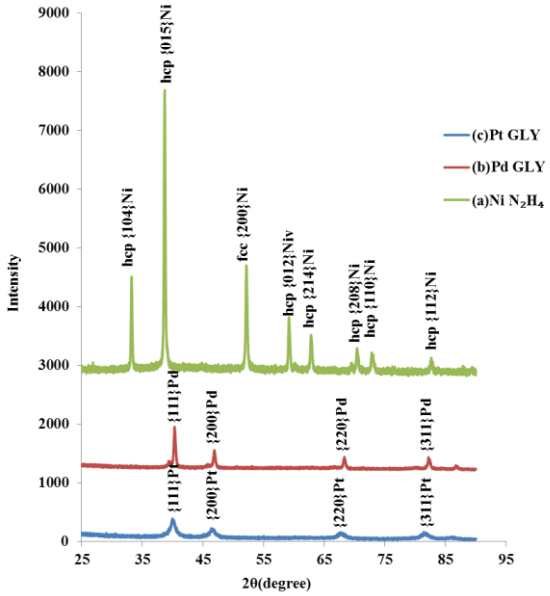

Figure 12: XRD Patterns of (a) Ni NPs stabilized with PVP/N_2H_4 at 90 °C, 2h; (b) Pd NPs (c) Pt NPs stabilized by PVP/GLY at 160 °C, 2h

Whereas, the diameter of PVP/GLY stabilized Pd nanoparticles (Figure 12b) based on the {111} diffraction planes was 25.75 nm, with a lattice spacing of 2.23 Å. In comparison, the average particle size obtained from TEM measurements was 18.28±5.72 nm. The four prominent *p*-XRD peaks appeared at 2ϑ reflections of 40.15°, 46.79°, 68.16° and 82.10° which were indexed to {111}, {200}, {220} and {311} face-centered cubic structure of Pd [51]. Similarly, Pt nanoparticles stabilized with PVP/GLY (Figure 12c) showed four peaks at 2ϑ reflections of 39.81°, 46.29°, 67.14° and 81.00° which were also indexed to {111}, {200}, {220} and {311} planes of fcc structure of Pt [52]. The particle size was 8.6 nm, and a lattice constant of 2.25 Å.

4. Conclusion

The synthesis of monometallic nanoparticles by wet chemical reduction and precipitation from aqueous and non-aqueous solutions was successfully carried with inorganic precursors stabilized or capped by polyvinylpyrrolidone, dodecanethiol or trisodium citrate. Characterization of the nanoparticles using optical spectroscopy showed the absence of peaks at 378 and 460 nm which indicates the reduction of Pt(IV), but Pd and Pt sols show broader absorption over the entire range of wavelength scanned. Generally, two major emission bands of PVP/polyol capped metallic sols were observed with strong emission peak between 400-417 nm reminiscent of Co, Ni and Ru nanoparticles excited at 340-360 nm, the strong emission band indicates the occurrence of S_1-S_o transition which can be said to be due to stoke's shift. The TEM images of Co NPs showed the formation of ethyleneglycol based nanosphere with an average diameter of 11.23±3.82 nm but the pentaerythritol based pseudo-cubic structures has an average diameter of 33.43±9.55 nm, which were corroborated by the absorption spectral measurement. The *p*-X-ray diffraction showed the existence of fcc with nearly pure crystalline phases for Pd and Pt NPs, while the hcp phase was predominant in Ni NPs.

Acknowledgements

The authors thank the National Research Foundation (NRF), South Africa through the South African Research Chair Initiative (SARChI) program for financial support.

References

[1] K. Patel, S. Kapoor, D. P. Dave, T. Mukherjee, J. Chem. Sci. **117**, 311 (2005).
[2] F. Zhang, Y. Pi, J. Cui, X. Zhang, N. Guan, J Phys Chem C **111**, 3756 (2007).
[3] P. V. Kamat, J Phys. Chem. B **106**, 7729 (2002).
[4] L. M. Liz-Marzan, Langmuir **22**, 32 (2006).
[5] P. Mukherjee, A. Ahmad, D. Mandal, S. Senapati, S. R. Sainkar, M. I. Khan, R. Parishcha, P. V. Ajaykumar, M. Alam, R. Kumar, M. Sastry, Nano Lett **1**, 515 (2001).
[6] R-X. Dong, W-C. Tsai, J-J. Lin, Eur. Polym. J. **47**, 1383 (2011).
[7] M. Ueji, M. Harada, Y. Kimura, J. Colloid Interf. Sci. **322**, 358 (2008).
[8] A. Chen, P. HolteHindle, Chem. Rev. **110**, 3767 (2010).
[9] C. Bianchini, P. K. Shen, Chem. Rev. **109**, 4183 (2009).
[10] N. V. Long, T. D. Hien, T. Asaka, M. Ohtaki, M. Nogami, Inter. J. hydrogen energy **36**, 8478 (2011).
[11] T.K. Sau, A.L. Rogach, Adv. Mater. **22**(16) 1781 (2010).
[12] A. R. Tao, S. Habas, P. Yang, Small **4**(3) 310 (2008).
[13] C. M. Niemeyer, Angew. Chem. Int. Edit. **40**(22) 4128 (2001).
[14] T-H. Trana, T-D. Nguyen, Colloid Surface B: **88**, 1 (2011).
[15] Y-Y Feng, J-H. Ma, G-R. Zhang, G. Liu, B-Q. Xu, Electrochem. Commun. **12**, 1191 (2010).
[16] C.L. Lee, C.C. Wan, Y.Y. Wang, Adv. Funct. Mater. **11**, 344 (2001).
[17] C.J. Lee, Y.C. Huang, C.C. Wan, Y.Y. Wang, Y.J. Ju, L.C. Kuo, J.C. Oung, J. Electrochem. Soc. **152**, C520 (2005).
[18] N. A. Frey and S. Sun, Magnetic Nanoparticle for Information Storage Applications. In C. Altavilla, E. Ciliberto. (Eds.). Inorganic Nanoparticles: Synthesis, Application, and Perspective, (pp 33-68), CRC Press, New York (2011).
[19] S. Kiadambi, M. L. Bruening, Chem. Mater. **17**, 301 (2005).
[20] N. Toshima, T. Takahashi, H. Hirai, Chem. Lett.**15**, 35 (1986).
[21] S. K. Filippov, J. Panek, P. Stepanek, Polymeric Nanoparticles Stabilized by Surfactants: Controlled Phase Separation Approach, In A. A. Hashim (Ed.). Smart Nanoparticles Technology, (pp 221-241), InTech., Croatia (2012).
[22] Y. W. Lee, M. Kim, Z. H. Kim, S. W. Han, J. Am. Chem. Soc. **131**, 17036 (2009).
[23] J. A. Adekoya, E. O. Dare, M. A. Mesubi, A. A. Nejo, H. C. Swart, N. Revaprasadu, Res. Phys. **4**, 12 (2014).
[24] X. Teng, H. Yang, Nano Lett. **5**, 885 (2005).
[25] M. Hoffman, S. Martin, W. Choi, D. Bahnemann, Chem. Rev. **95**, 69 (1995).
[26] R. V. Kumar, Y. Diamant, A. Gedanken, Chem. Mater. **12**, 2301 (2000).
[27] A. Gulino, P. Dapporto, P. Rossi, I. Fragala, Chem. Mater. **15**, 3748 (2003).
[28] D. I. Michael, D. B. Buchholz, W. H. Alexander, P. H. C. Robert, J. M. Tobin, P. Natl. Acad. Sci. USA **105**, 2783 (2007).
[29] B. Sarkar, K. Chakrabarti, K. Das, S. K. De, J. Phys. D: Appl. Phys. **45**, 505304 (10pp) (2012).
[30] J. S. Wilson, A. Kohler, R. H. Friend, M. K. Al-Suti, M. R. A. Al-Mandhary, M. S. Khan, P. R. Raithby, J. Chem. Phys. **113**, 7627 (2000).
[31] A. Kohler, J. S. Wilson, R. H. Friend, M. K. Al-Suti, M. S. Khan, A. Gerhard, H. Bassler, J. Chem. Phys. **116**, 9457 (2002).
[32] R. Fischer, S. Schuppler, N. Fischer, Th. Fauster, W. Steinmann, Phys. Rev. Lett. **70**, 654(1993).
[33] J. Gao, J. Fu, C. Lin, J. Lin, Y. Han, X. Yu, C. Pan, Langmuir **20**, 9775 (2004).

[34] B. E. Conway, Electrochemical Supercapacitors: Scientific Fundamentals and Technological Applications, Kluwer-Plenum, New York (1999).
[35] P. Liska, N. Vlachopoulos, M. K. Nazeeruddin, P. Comte, M. Graetzel, J. Am. Chem. Soc. **110**, 3686 (1988).
[36] P. K. Jain, K. S. Lee, I. H. El-Sayed, M. A. El-Sayed, J. Phys. Chem. *B* **110** , (14) 7238 (2006).
[37] S. Baset, H. Akbari, H. Zeynali, M. Shafie, Dig. J. Nanomater. Bios. **6**, 709 (2011).
[38**]** M. Thiry, K. Boldt, M. S. Nikolic, F. Schulz, M. Ijeh, A. Panicker, T. Vossmeyer, H. Weller, *ACS Nano* **5,** 4965 (2011).
[39] W. Lou, M. Chen, X. Wang, W. Liu, Mater. Lett. **61**, 3612 (2007).
[40] J.A. Adekoya, S. Mlowe, E. O. Dare, M. A. Mesubi, N. Revaprasadu, Superlattice Microst. **78**, 97 (2015).
[41] K. Konga, M. Hirasawa, Nanotechnology **24**, 375602 (2013). doi:10.1088/0957-4484/24/37/375602
[42] R. F. Wang, H. Wang, B. X. Wei, W. Wang, Z. Q. Lei, Inter. J. Hydrogen Energ. **35**, 10081 (2010).
[43] N. Wenxin, Y. Guobao, Review: Nano Today **6**, 265 (2011).
[44] B. P. Vinayan, R. I. Jafri, R. Nagar, N. Rajalakshmi, K. Sethupathi, S. Ramaprabhu, Int. J. Hydrogen Energ. **37** 412 (2012).
[45] I. Srnova-Sloufova, F. Lednicky, A. Gemperle, J. Gemperlova, Langmuir **16**, 9928 (2000).
[46] T. Tao, A. M. Glushenkov, H. Liu, Z. Liu, X. J. Dai, H. Chen, S. P. Ringer, Y. Chen, J. Phys. Chem. C **115**, 17297 (2011).
[47] M. C. Morris, H. F. McMurdie, E. H. Evans, B. Paretzkin, H. S. Parker, N. C. Panagiotopoulos, Section 18-Data for 58 Substances, International center for diffraction data, Camden R. Hubbard (Ed.), U.S. Department of Commerce, Malcolm Baldrige, Secretary National Bureau of Standards, Issued October 1981.
[48] Y. Chen, D-L. Peng, D. Lin, X. Luo, Nanotechnology **18,** 505703 (6pp) (2007).
[49] J. Sehested, J. A. P. Gelten, I. N. Remediakis, H. Bengaard, J. K. Nørskov, pressures, J. Catal. **223**, 432 (2004).
[50] V. Tzitzios, G. Basina, M. Gjoka, V. Alexandrakis, V. Georgakilas, D. Niarchos, N. Boukos, D. Petridis, Nanotechnology **17**, 3750 (2004).
[51] Y. Suo, I-M. Hsing, Electrochim. Acta **56**, 2174 (2011).
[52] L. Chen, W. Zhao, Y. Jiao, X. He, J. Wang, Y. Zhang, Spectrochim. Acta A **68**, 484 (2006).